Absorb/Transmit Broadband Type Frequency Selective Surface

José Jaime G. P. Neto[1] , Antonio Luiz P. S. Campos[1] , Ruann Victor de A. Lira[1] , Alfredo Gomes Neto[2] , Maurício W. B. Silva[3]

[1] *Communication Engineering Department, Federal University of Rio Grande do Norte (UFRN), Rio Grande do Norte, Brazil, alpscampos@gmail.com, josejaimegpneto@gmail.com, ruannvictor@gmail.com*
[2] *Federal Institute of Education, Science and Technology of Paraíba (IFPB), Campus João Pessoa, Paraíba, Brazil, alfredogomesjpa@gmail.com*
[3] *Telecommunications Engineering Department, Fluminense Federal University, Rio de Janeiro, Brazil, mauriciobenjo@id.uff.br*

Abstract— **Frequency Selective Surfaces (FSS) are increasingly being used in telecommunications systems due to the numerous advantages presented by this sort of structure, among them low cost, ease of fabrication, and low profile stand out. This work reports the design, fabrication, and characterization of a multilayer frequency-selective absorber (FSA) for broadband operation. The proposed structure shows an absorption performance (operating in the frequency range between 2 GHz and 6 GHz) within the transmission band. The absorber consists of cascaded frequency selective surfaces, which are composed of both conductive square loops, which reflect incident signals, and resistive ones, which act as an absorbing layer. To verify the absorbing structure performance, full-wave numerical simulations and measurements are presented. The measured results are in good agreement with the numerical ones and show that the design performs absorption above 80% within the range of 2.48 GHz to 6.13 GHz, which verifies the project properties. Besides that, numerical results show that the proposed absorber has a proper response under oblique incidence up to $30°$.**

Index Terms— Frequency Selective Surfaces, Multilayer Absorber, Broadband

I. INTRODUCTION

The expansion of wireless communications has caused an increase in the use of the frequency spectrum and, as a result, there is an increase in electromagnetic interference problems, mainly in unlicensed bands. Added to this, there are problems arising from interference due to multipath in mobile communications. Microwave absorbers can be used to reduce problems caused by electromagnetic interference and by multipath [1]–[8].

A controllable electromagnetic disturbance environment is an important issue in the development of radar electromagnetic wave absorption structures and problems of interference and electromagnetic compatibility. Electromagnetic wave absorption refers to the ability of a structure or material to attenuate the energy of an incident electromagnetic wave. The total control of the received radiation may be desirable since several phenomena are inherent to electromagnetic disturbances, such as polarization control, interference, spurious radiation, leakage, susceptibility, and multipath, to name a few [9]–[11]. Electromagnetic absorbers are structures suitable for this purpose.

Pyramidal absorbers are the most famous and used radar absorbing structures due to their high performance over a wide frequency range [12], [13]. For environments where space demand is not

an important factor, the volume of pyramidal absorbers does not become a critical issue. In other applications (*e. g.* radar cross-section reduction or electromagnetic compatibility), the thickness and weight of these absorbers are not suitable.

Electromagnetic absorbers are divided into different types such as pyramidal graphite absorbers, ultrathin, nanomagnetic ingredients, and so on. The pyramidal absorbers used in anechoic chambers have low levels of reflection but are bulky. As a result, it is impossible to be used in all applications. Furthermore, pyramidal absorbers are generally used indoors due to their sensitivity to dust, humidity, and temperature [14].

An alternative to reducing the bulk and weight of an absorber is to use both resistive and metallic frequency selective surfaces printed on dielectric materials. Usually, to obtain broadband responses, FSS should be used in multilayer dielectric structures [15]–[17]. This can lead to an increase in volume and weight, but the final structure is typically smaller compared to Pyramidal and Jaumann absorbers in general.

Several works in the literature propose the use of multilayer FSS to design broadband-type absorbers [18], [19]. In [18], the authors proposed a simple, fast, and efficient method for designing broadband absorbers. The authors proposed to modify the analog circuit absorber method without changing the bandwidth. The proposed absorber contains three layers, with a total thickness of 15.1 mm, and has proved to be a better solution than the Jaumann absorber.

In [20] and [21], the authors proposed the design of broadband microwave absorbers incorporating resistive FSS in multiple dielectric layers. A binary coded genetic algorithm (GA) was used to determine the resistive unit cell shape, the material and thickness of each layer, the FSS periodicity, as well as the number of dielectric layers. Finally, a full ground plane was placed in the last layer.

The common point among all the works presented so far is the use of a full ground plane in the last layer. This makes the multipath problem worse in the vicinity of the structures in which these absorbers are inserted. Hence, this work proposes an absorber composed of both resistive and metallic FSS properly spaced in multiple layers for wideband absorption. The use of metallic FSS rather than a full ground plane will allow the absorber to not only maintain broadband absorption but also avoid multipath problems.

The Jaumann absorber consists of two or more resistive screens and a conductive ground plane. These structures are spaced by a distance of a quarter-wavelength, whose main function is to increase the absorption bandwidth. The greater the number of resistive layers, the greater the absorption bandwidth. However, this absorber presents two problems, the first one is that the fixed quarter-wavelength separation can make it very bulky, depending on the desired absorption bandwidth. The second one is that it will reflect all signals outside the absorption frequency range, which can lead to multipath problems in the vicinity of the structure, in addition to preventing the transmission of signals outside the absorption range.

Considering the previous discussion, this work proposes a multilayer broadband frequency-selective absorber, as a Jaumann structure. Considering the absorptivity above 80% as a reference absorption level, the proposed structure covers the 2.4 to 6 GHz frequency band, absorbing the entire ISM and UNII band, as well as the 5G band at 3.5 GHz. The novelties of the proposed absorber are the simple design, compact size compared to traditional Jaumann absorbers, and without the use of a full metallic ground plane. Therefore, the structure absorbs the frequency bands of interest, allowing the other frequencies

to pass through.

II. PROPOSED STRUCTURE

To overcome the problems discussed about the Jaumann absorber, we propose a structure that replaces both the resistive screens and the full conductive plane by resistive FSS and conductive FSS, respectively. To achieve the desired absorption band, two resistive and two conductive FSS are used, all composed of square loops. The use of two resistive and two conductive layers is justified by the fact of obtaining more precision in the structure frequency response. Furthermore, the square loop is known for its angular stability and polarization independence. Fig.1(a) illustrates the proposed absorber and Fig.1(b) illustrates the geometry of the unit cells used in the layers.

The metallic layers use FR-4 as substrate, with thicknesses h_1 of 1.6 mm, a dielectric constant of 4.4, and a loss tangent of 0.02. On the other hand, the resistive layers have a surface resistance of 50 $\Omega/\square$, FR-4 as substrate with thicknesses h_2 of 2.0 mm. The resistive FSSs are fabricated on OHMEGAPLY® dielectrics covered with a thin film of nickel-phosphorus resistive material. The conductive FSS were manufactured with a corrosion process using an iron perchloride solution. The resistive FSS manufacturing process begins with the corrosion of the OhmegaPly resistive FR4 plate using an iron perchloride solution. After this process, the FR4 plate must be exposed to an alkaline solution composed of 250 grams per liter of sulfate of hydrated copper penta and 3 to 5 milliliters per liter of sulfuric acid. This solution must be kept at 90°C to be applied to the FR4 plate. Finally, the plate is corroded again using iron perchloride.
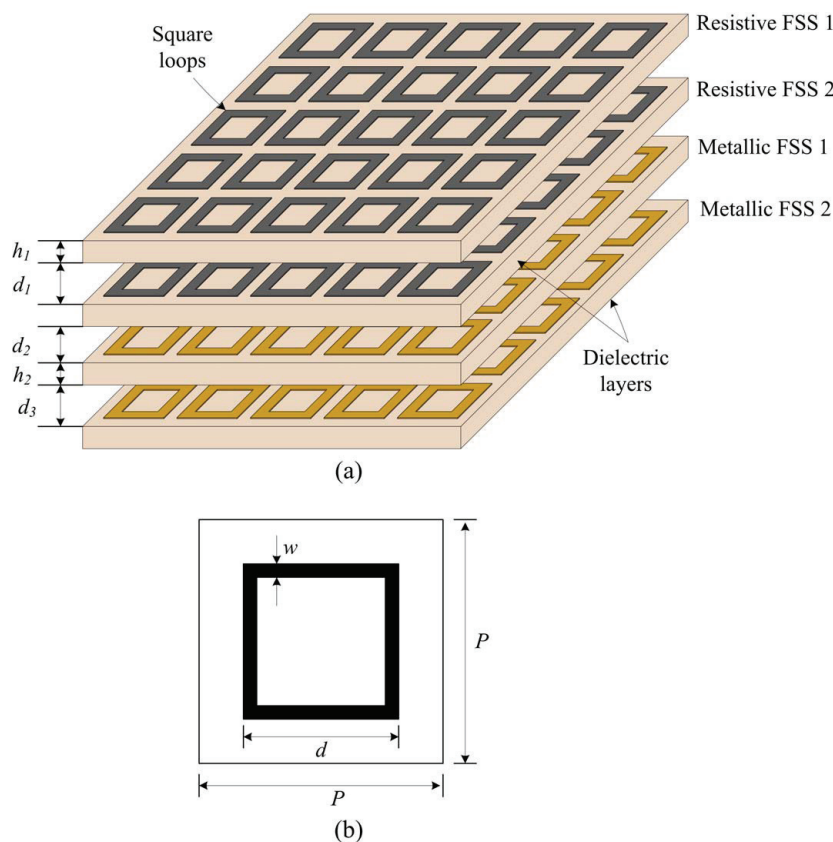

(a)

(b)

Fig. 1. Proposed absorber: (a) cascade structure and (b) unit cell geometry.

We used a parametric analysis, with the HFSS software, to optimize the physical dimensions of the conductive square loops. The initial dimensions were $\lambda/4$, for dimension d (square loop side), for the resonant frequencies of 3.0 GHz and 5.5 GHz. So, for the first conductive FSS the initial dimensions were d_{c1} = 13.6 mm ($\lambda/4$ for 5.5 GHz) and w_{c1} = 2 mm (for fabrication purpose). For the second conductive FSS the initial dimensions were d_{c2} = 25 mm ($\lambda/4$ for 3.0 GHz) and w_{c2} = 2 mm. After the parametric optimization, the first conductive FSS has square loops with dimensions d_{c1} = 17.8 mm and w_{c1} = 3 mm. The second conductive FSS has square loops with dimensions d_{c2} = 21.5 mm and w_{c2} = 2.2 mm. The first resistive FSS has loops with dimensions d_{r1} = 17.8 mm and w_{r1} = 4 mm. Finally, the second resistive FSS has loops with dimensions d_{r2} = 21.5 mm and w_{r2} = 3 mm.

In this article, to obtain a more compact structure, the effect of spacing on the transmission and reflection coefficients under normal incidence is investigated. All simulated results were obtained with the HFSS commercial software and only the absorption was obtained with (1). Therefore, Fig. 2 shows the S-parameters for different spacing values, d_1, d_2, and d_3, for TE polarization. It is observed that the transmission coefficient (S_{21}) has low variation. On the other hand, the reflection coefficient (S_{11}) presents a shift in the operating band, changing from 3 to 5 GHz (for 5 mm) to 4 to 6.7 GHz (for 10 mm).

To analyze this effect, we obtained the absorptivity curves (see Fig. 3) for the two spacings, using (1):

$$A = 1 - \Gamma(\omega) - T(\omega) \tag{1}$$

where $R(\omega) = |R_{xx}|^2 + |R_{yx}|^2$ is the reflected power and $T(\omega) = |T_{xx}|^2 + |T_{yx}|^2$ is the transmitted power. The co- and cross-polarized components are represented by '*xx*' and '*yx*', respectively.
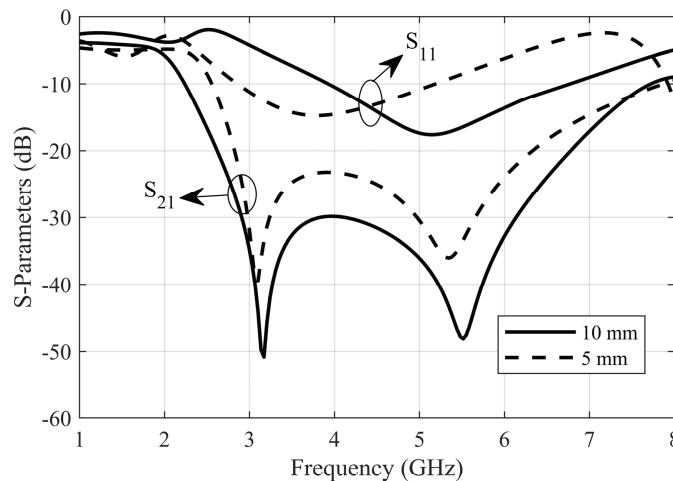

Fig. 2. S-parameters for gaps of 5 mm and 10 mm.

From Fig. 3, it is observed that for a spacing of 10 mm the absorptivity remains above 80% for the frequency range 3.5 to 7.1 GHz, while for the 5 mm spacing, the absorptivity was changed to 2.5 to 5.9 GHz, which meets the requirements for the ISM, 5G at 3.5 GHz and UNII bands.
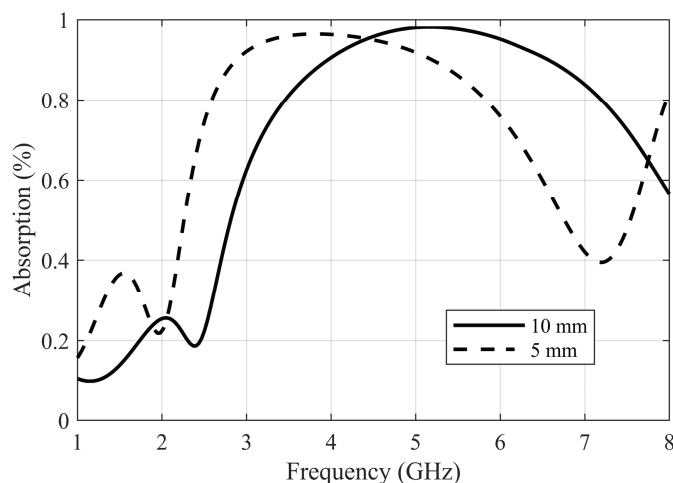
Fig. 3. Absorption comparison among different gaps.

To investigate the angular stability and polarization independence, the structure was analyzed under oblique incidence up to 30°. Fig. 4 illustrates the results for angular variation and vertical polarization. As can be seen, the absorption band of interest remains almost unchanged, ensuring absorption of the frequencies of interest. For horizontal polarization, it can be seen that a second narrow absorption band appears from 20°, but the absorption band of interest is almost the same (seen Fig. 5). Furthermore, the second absorption band is around 7 GHz, which does not affect most indoor applications.
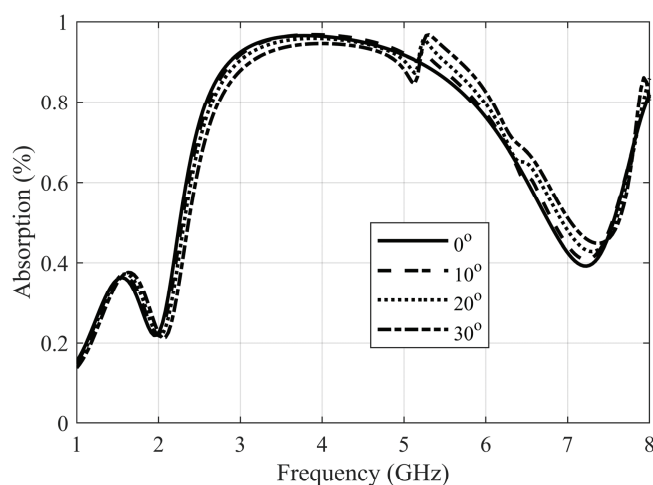

Fig. 4. Absorptivity under normal incidence and oblique incidence for TE polarization.

Fig. 6 illustrates the surface current distribution in the conductive FSSs as well as the electric field distribution in the resistive FSSs, for the frequency of 4.5 GHz, which is the central frequency of the absorption band. It is possible to observe that both the induced surface current distributions and the electric field distributions are symmetrical, which guarantees angular stability for the structure. Furthermore, it is possible to notice the presence of induced surface currents in the two conducting loops, at the frequency of 4.5 GHz [Figs. 6(a) and (b)], which guarantees the blocking of transmission of electromagnetic waves at that frequency. On the other hand, the electric field is dissipated in the resistive FSSs [Figs. 6(c) and (d)], avoiding reflections at the absorption frequencies. This demonstrates that the proposed absorber prevents transmission and reflection in the proposed frequency range.
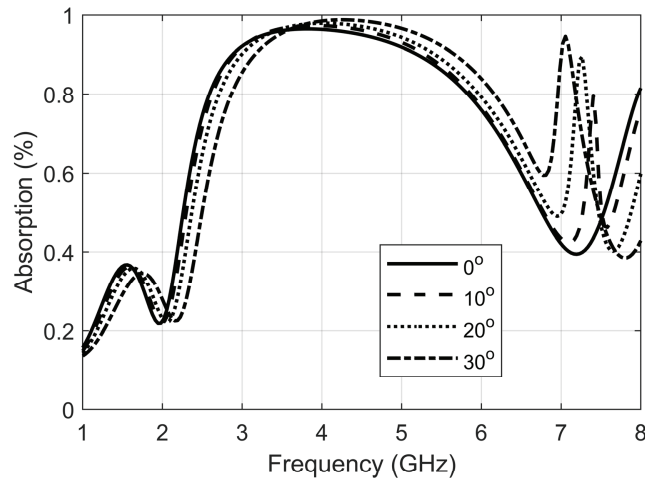
Fig. 5. Absorptivity under normal incidence and oblique incidence for TM polarization.
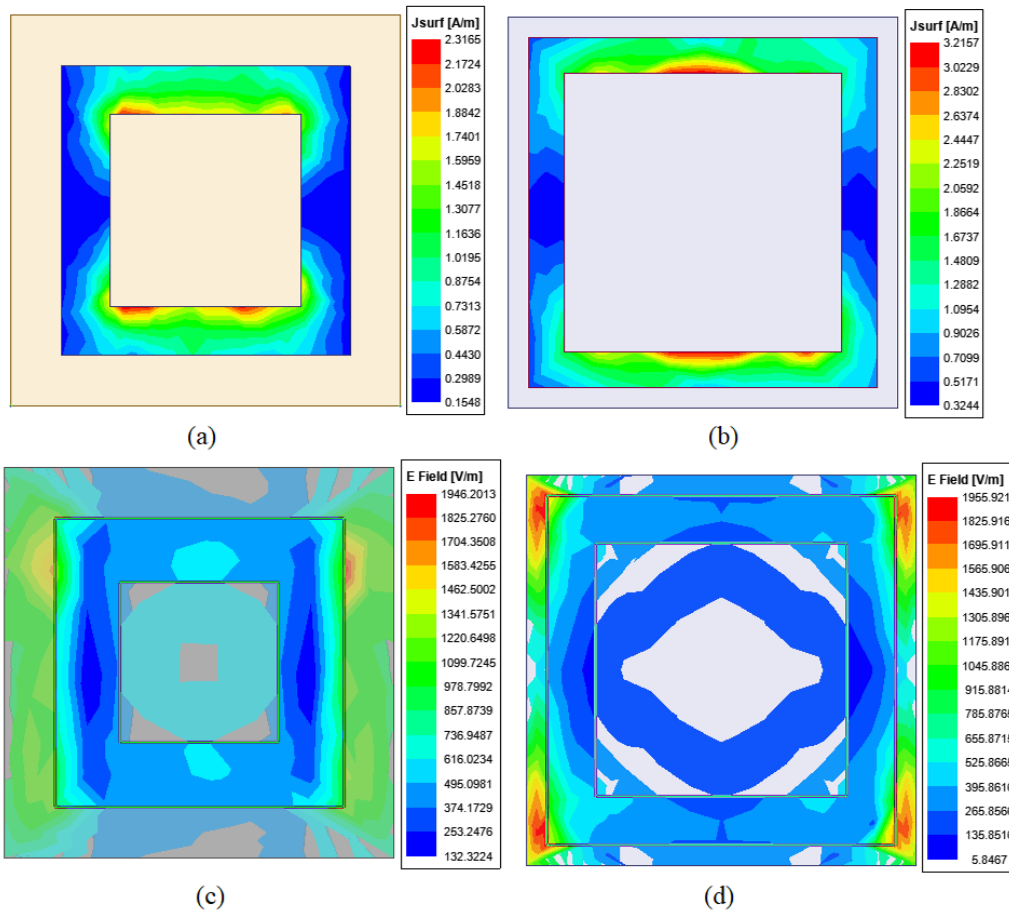

Fig. 6. Simulated surface current density and electric field distribution of the proposed absorber at 4.52 GHz.

III. EXPERIMENTAL VERIFICATION

To validate the numerical results and experimentally verify the absorption characteristics of the proposed structure, a 200 x 200 mm (7 x 7 unit cells) sample was fabricated. The fabricated sample and the measurement setups photographs are shown in Fig. 7. The proposed absorber was measured using the free-space method, at S- and C-bands. The measurement setup consisted of a vector network

analyzer (model N5230A from Keysight) and ultra-wideband horn antennas (model SAS-571 from A. H. Systems, operating from 700 MHz to 18 GHz) with 14 dBi gain. For normal incidence measurement, the antennas were connected to the network analyzer and placed at a distance of 1.3 m from the prototype [see Fig. 7(b)]. The measured transmission response was normalized to an open window and then the proposed absorber was placed in the window to measure the transmission through it. Furthermore, the device under test (DUT) was inserted into a frame of radar absorbing material (RAM) having a square window measuring 200 x 200 mm, as illustrated in Fig. 7(b) and (c). The transmission and reflection coefficients were measured using the configurations illustrated in Figs. 8 and 9, respectively. The setup is shown in Fig. 9 and it limits the angular incidence measurements.
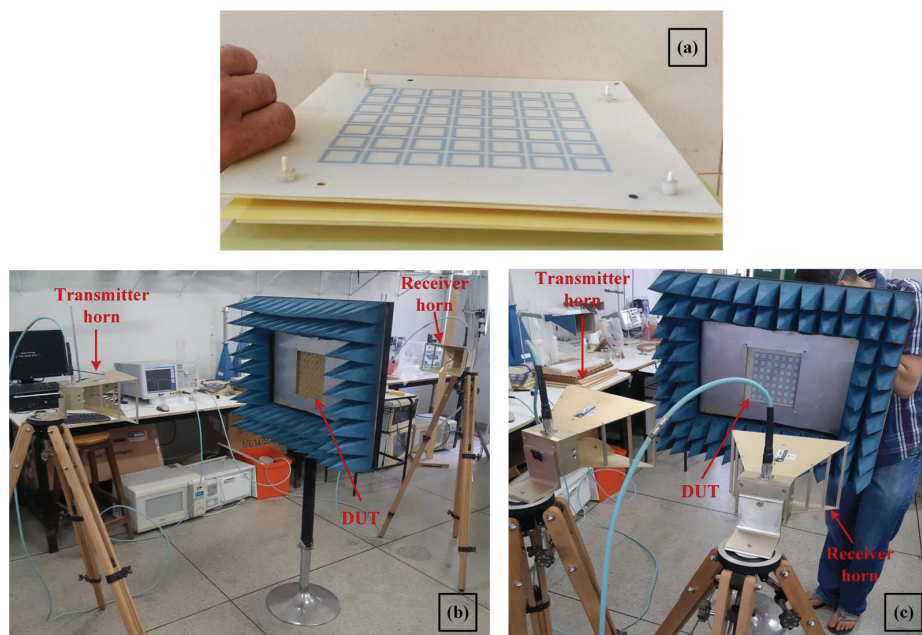

Fig. 7. Photograph of (a) fabricated prototype, (b) transmission coefficient and (c) the reflection coefficient.
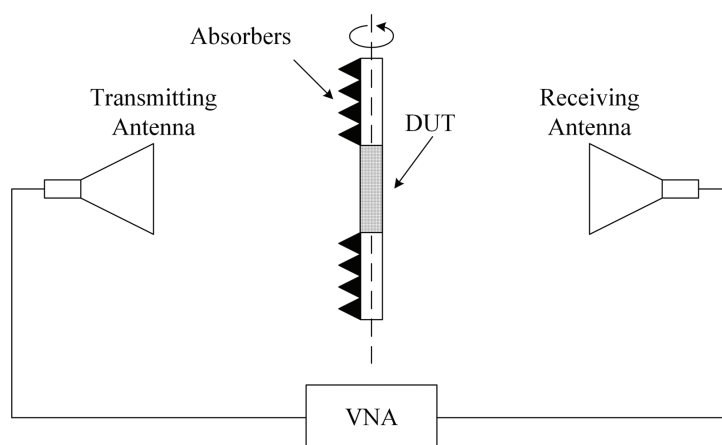

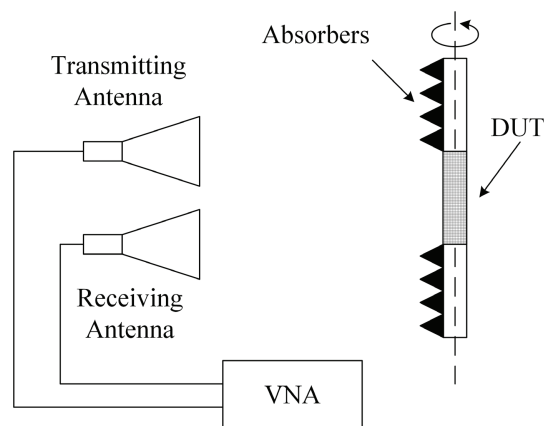Fig. 8. Transmission coefficient measurement setup.

Fig. 9. Reflection coefficient measurement setup.

Initially, the transmission coefficients of the conductive FSS were measured to validate the project and verify the frequency responses. Fig. 10 shows the comparison between simulated and measured results for the first conductive FSS, which was designed to operate in the 2 to 4 GHz frequency range. Simulated results show that the resonance frequency occurs at 3.13 GHz and the -10 dB stop-band goes from 2.13 GHz to 4.07 GHz. The measured results show that the resonant frequency occurs at 3.37 GHz and the -10 dB stop-band goes from 2.36 GHz to 4.18 GHz. There is a good agreement between the results, showing the viability of the structure.

Fig. 11 shows the comparison between the simulated and measured results for the second conductive FSS, designed to block signals in the 4.5 to 6.5 GHz frequency band. The simulated results show that the resonant frequency occurs at 5.62 GHz (5.68 GHz in measurements) and the -10 dB stop-band goes from 4.48 GHz to 6.55 GHz (3.72 GHz to 6.55 GHz in measurements). As it can be observed, the results also show good agreement, which demonstrates the feasibility of the second reflective FSS design.
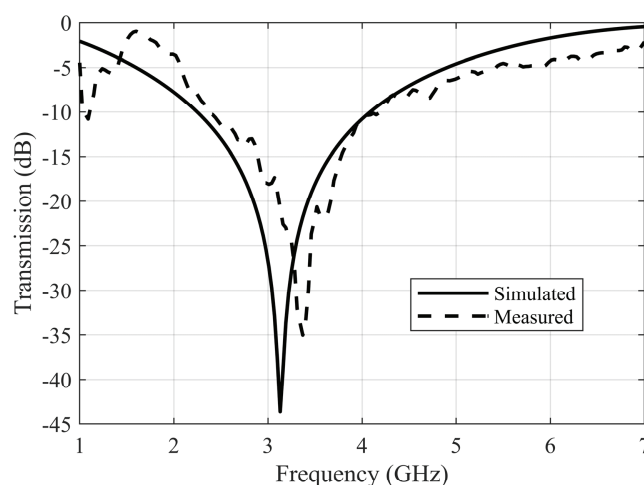

Fig. 10. Comparison between simulated and measured results of the transmission coefficient for the first conductive FSS.

Measurements of the final assembled structure were carried out to validate the design in terms of transmission and reflection coefficients and absorption band. Fig. 12 shows the comparison between simulated and measured results for the transmission coefficient of the absorber structure. The simulated results show that the stop-band goes from 2.48 GHz to 7.00 GHz, against a stop-band from 2.44 GHz to

6.92 GHz for the measurement results, these values being considered for – 10 dB. It can be concluded that the agreement between numerical results and free-space measurements is reasonably good over the entire analyzed frequency range.
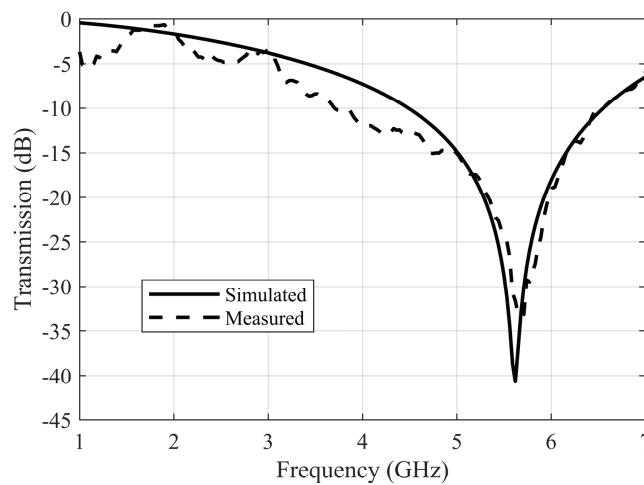

Fig. 11. Comparison between simulated and measured results of the transmission coefficient for second conductive FSS.
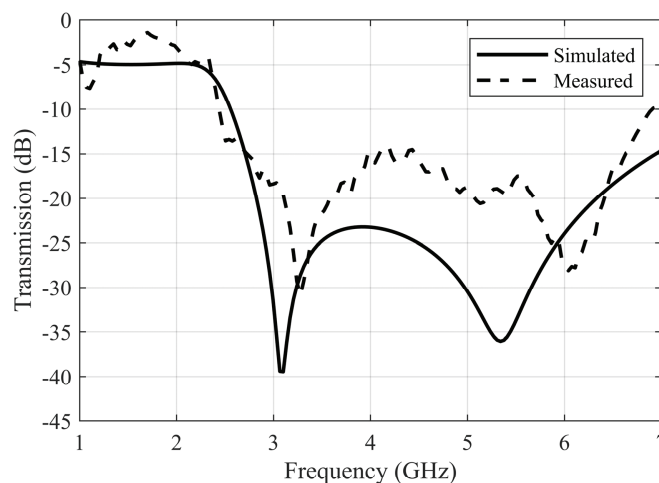

Fig. 12. Comparison between simulated and measured results of the absorber transmission coefficient.

The simulated reflection coefficient results show that the stop-band goes from 2.94 GHz to 5.21 GHz, against a band that goes from 2.89 GHz to 5.98 GHz for the measured results, this value being also considered for −10 dB. These results are in good agreement with each other, demonstrating that the design is very close to meeting the intended band in terms of the reflection coefficient. These results are illustrated in Fig. 13.
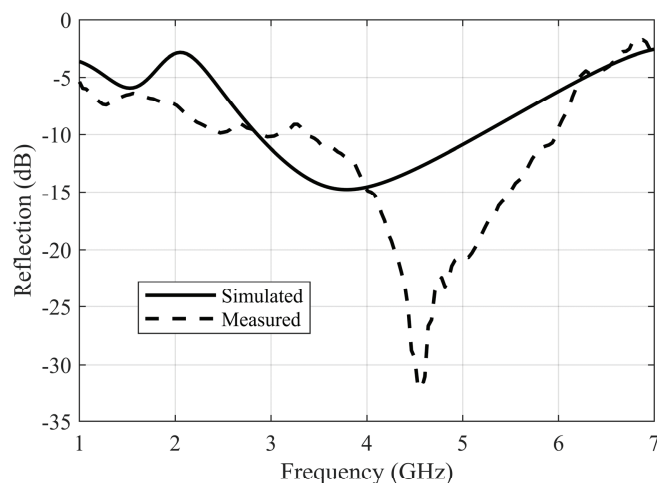
Fig. 13. Comparison between simulated and measured results for the absorber reflection coefficient.

Fig. 14 shows the simulated and measured absorptivities of the proposed structure under normal incidence. There is a good agreement between the results, in which both presented a high level of absorption across the analyzed band. The frequency band over which the absorption is above 80%, which is the absorption limit considered in this study, is from 2.68 GHz a 5.87 GHz in the simulations (2.48 GHz to 6.13 GHz in measurements), showing a wide absorption band and covering almost completely the S-band and part of the C-band. The measured results show that an efficient absorption is achieved with fractional bandwidth of 84.7% and with an average absorption ratio of 92.2%. Furthermore, the thickness of the proposed absorber is, in terms of the wavelength at the lowest measured frequency (2.48 GHz), $0.18\lambda_L$, and the periodicity P is $0.19\lambda_L$, which means that both thickness and periodicity are smaller than the wavelength. Some deviations are noted in Figs. 12 and 13. These deviations are because we did not use an anechoic chamber to realize the measurements. However, the most important parameter is the Absorption, illustrated in Fig. 14, and for it the results are in good agreement, with little deviation.
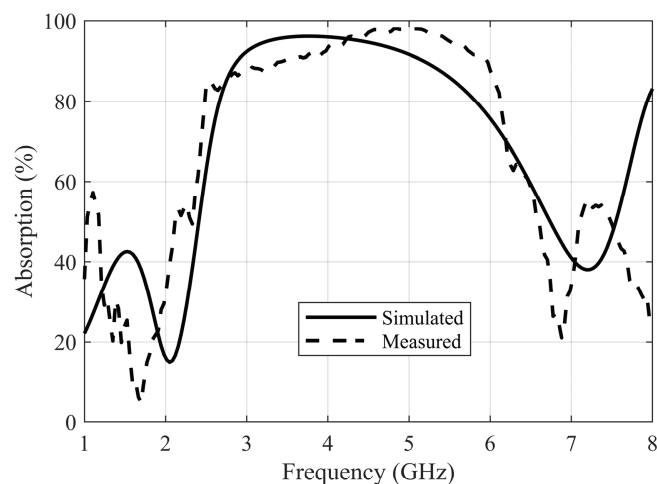

Fig. 14. Comparison between simulated and measured absorption results.

From the presented results, it can be seen that the proposed structure presents a broadband operation, covers the entire ISM ($2.4 - 2.4935$ GHz), 5G at 3.5 GHz and UNII ($5 - 6$ GHz) bands, without blocking

the other frequencies, avoiding multipath propagation in the vicinity where the absorber is installed, which does not happen with the structures proposed in the literature.

IV. CONCLUSION

A wideband, polarization-insensitive, and angular stability absorber was proposed in this paper. Through a combination of resistive and conductive FSS in cascade, composed of square loops, it was possible to obtain a wideband frequency-selective absorber. This has, to the best of the authors' knowledge, is the first reported broadband absorber without a full ground plane and using FSS. The numerical results show that the proposed absorber exhibits absorption up to an incidence angle of 30°. Furthermore, numerical and measurement results show that the proposed structure can absorb signals in a frequency range from 2.4 to 6.13 GHz. The measured results show good agreement with the numerical ones, with absorption above 80% in the entire analyzed frequency range. The proposed structure can absorb signals for the entire ISM band (2.4 – 2.4835 GHz), 5G at 3.5 GHz and UNII (5 – 6 GHz), without blocking the other frequencies, avoiding multiple paths in the vicinity where the absorber is installed, which does not happen with the structures proposed in the literature.

REFERENCES

[1] M. Gustafsson, A. Karlsson, A. Rebelo, and B. Widenberg, "Design of frequency selective windows for improved indoor outdoor communication," *IEEE Transactions on Antennas and Propagation*, vol. 54, pp. 1897–1900, 2006.

[2] F. Che Seman and R. Cahill, "Frequency selective surfaces based planar microwave absorber," in *Progress in Electromagnetics Research Symposium*, pp. 906–909, 2012.

[3] B. C. J. C. Bennett and G. E. Crossley, "Characterisation of microwave four-parameter materials and its application in wideband radar absorber design," in *IEE Proceedings - Radar, Sonar and Navigation*, pp. 337–340, 1994.

[4] F. Che Seman and R. Cahill, "Frequency selective surfaces based planar microwave absorber," in *Progress in Electromagnetics Research Symposium*, pp. 906–909, 2012.

[5] Z. Y. M. A. H. B. P. Chen, M. Farhat and D. Erricolo, *Recent Topics in Electromagnetic Compatibility: Artificial Surfaces and Media for Electromagnetic Absorption and Interference Shielding*. IntechOpen, 2021.

[6] K. S. T. Beeharry, R. Yahiaoui and H. H. Ouslimani, "A dual layer broadband radar absorber to minimize electromagnetic interference in radomes," *Scientific Reports*, vol. 8, pp. 1–9, 2018.

[7] A. N. T. M. T. Yamane, K. Nagata, "Wide-band electromagnetic wave absorber panel for multipath interference reduction in urban areas," *Journal of The Institute of Image Information and Television Engineers*, vol. 63, pp. 1659–1666, 2009.

[8] X. B. R. H. K. G. R. S. K. L. Xin Zhou, Zhangdui Zhong and X. Guo, "Impacts of absorber loadings on simulating the multipath channel in a reverberation chamber," *International Journal of Antennas and Propagation*, vol. 2017, pp. 1–7, 2017.

[9] W. P. C. H. O. L. H. F. M. X. Gao, X. Han and T. J. Cui, "Ultrawideband and high-efficiency linear polarization converter based on double V-shaped metasurface," *IEEE Transactions on Antennas and Propagation*, vol. 63, pp. 3522–3530, 2015.

[10] C. R. Paul, *Introduction to Electromagnetic Compatibility*. Wiley-Interscience, 2006.

[11] A. T. L. P. F. Marra, J. Lecini and M. S. Sarto, "Electromagnetic wave absorption and structural properties of wide-band absorber made of graphene-printed glass-fibre composite," *Scientific Reports*, vol. 8, pp. 1–9, 2018.

[12] B. K. Chung and H.-T. Chuah, "Modeling of rf absorber for application in the design of anechoic chamber," *Progress in Electromagnetic Research*, vol. 43, p. 273–285, 2003.

[13] A. Fallahi and A. Enayati, "Modeling pyramidal absorbers using the fourier modal method and the mode matching technique," *IEEE Transactions on Electromagnetic Compatibility*, vol. 58, pp. 820–827, 2016.

[14] Z. H. F. M. Basravi, M. Maddahali and A. Ramezani, "Design of a novel ultra broadband single-layer absorber using double fractal square loops," in *2016 24th Iranian Conference on Electrical Engineering (ICEE)*, pp. 621–625, 2016.

[15] B. A. Munk, *Frequency Selective Surface: Theory and Design*. John Wiley & sons, 2000.

[16] R. L. Fante and M. T. McCormack, "Reflection properties of the salisbury screen," *IEEE Transactions on Antennas and Propagation*, vol. 36, pp. 1443–1454, 1988.

[17] L. J. D. Toit and J. H. Cloete, "Electric screen jauman absorber design algorithms," *IEEE Transactions on Microwave Theory and Techniques*, vol. 44, pp. 2238–2245, 1996.

[18] A. K. Zadeh and A. Karlsson, "Capacitive circuit method for fast and efficient design of wideband radar absorbers," *IEEE Transactions on Antennas and Propagation*, vol. 57, pp. 2307–2314, 2009.

[19] A. Kazemzadeh, "Nonmagnetic ultrawideband absorber with optimal thickness," *IEEE Transactions on Antennas and Propagation*, vol. 59, pp. 135–140, 2011.

[20] R. M. S. Chakravarty and N. R. Williams, "On the application of the microgenetic algorithm to the design of broadband microwave absorbers comprising frequency-selective surfaces embedded in multilayered dielectric media," *IEEE Transactions on Microwave Theory and Techniques*, vol. 49, pp. 1050–1059, 2001.

[21] S. Chakravarty, R. Mittra, and N. Williams, "Application of a microgenetic algorithm (MGA) to the design of broadband microwave absorbers using multiple frequency selective surface screens buried in dielectrics," *IEEE Transactions on Antennas and Propagation*, vol. 50, pp. 284–296, 2002.